

## MAGNETOHYDRODYNAMIC SIMULATION FROM THE CONVECTION ZONE TO THE CHROMOSPHERE

W. Schaffenberger<sup>1</sup>, S. Wedemeyer-Böhm<sup>1</sup>, O. Steiner<sup>1</sup>, and B. Freytag<sup>2</sup>

<sup>1</sup>Kiepenheuer-Institut für Sonnenphysik, 79104 Freiburg, Germany

<sup>2</sup>Los Alamos National Laboratory/Dep. of Phys. and Astron., Michigan State Univ., USA

### ABSTRACT

With the computer code CO<sup>5</sup>BOLD, a three-dimensional magnetohydrodynamic simulation of the integral layers from the convection zone to the chromosphere has been carried out. The MHD extension of CO<sup>5</sup>BOLD, which is a combination of an approximate Riemann solver with a constrained transport method, is briefly described. The simulation is intended to represent magnetoconvection in a quiet network-cell interior. The following preliminary new results are obtained: The chromospheric magnetic field is marked by strong dynamics with a continuous reshuffling of magnetic flux on a time scale of less than 1 min. Rapidly moving filaments of stronger than average magnetic field form in the compression zone downstream and along propagating shock fronts that are present throughout the chromosphere. These magnetic filaments that have a field strength rarely exceeding 40 G, rapidly move with the shock waves and quickly form and dissolve with them. The picture of flux concentrations that strongly expand through the photosphere into a more homogeneous, space filling chromospheric field remains valid. With the present new code, it became for the first time possible to extend simulations of magnetoconvection of the surface layers into the chromosphere.

Key words: Sun, chromosphere, MHD, magnetic fields, inter network.

### 1. THE NUMERICAL METHOD

The simulations were made with the CO<sup>5</sup>BOLD-code, which was recently extended to include magnetic fields. The code solves the coupled system of the equations of compressible magnetohydrodynamics in an external gravity field and non-local, frequency-dependent radiative transfer. The code was developed mainly by Bernd Freytag and Matthias Steffen based on long-term experience gathered with a previous radiation hydrodynamics code, designed to simulate two-dimensional solar convection. The main features of the code are the use of

a realistic equation of state, including partial ionization. Radiative transfer, hydrodynamics and additional turbulent diffusion are treated separately using operator splitting. Here, we only describe the MHD extension of CO<sup>5</sup>BOLD.

#### 1.1. The MHD equations

The ideal MHD equations describe the flow of an perfectly conducting fluid with zero viscosity and thermal conductivity and its interaction with a magnetic field. These equations express the conservation of mass, momentum, energy and magnetic flux. Including gravity, they can be written in conservative form as

$$\frac{\partial \mathbf{U}}{\partial t} + \nabla \cdot \mathbf{F} = \mathbf{S}, \quad (1)$$

where the vector of conserved variables  $\mathbf{U}$ , the flux tensor  $\mathbf{F}$  and the source terms due to gravity  $\mathbf{S}$  are

$$\mathbf{U} = \begin{pmatrix} \rho \\ \rho \mathbf{v} \\ \mathbf{B} \\ E \end{pmatrix}, \quad (2)$$

$$\mathbf{F} = \begin{pmatrix} \rho \mathbf{v} \\ \rho \mathbf{v} \mathbf{v} + \left( p + \frac{\mathbf{B} \cdot \mathbf{B}}{8\pi} \right) \mathbf{I} - \frac{\mathbf{B} \mathbf{B}}{4\pi} \\ \mathbf{v} \mathbf{B} - \mathbf{B} \mathbf{v} \\ \left( E + p + \frac{\mathbf{B} \cdot \mathbf{B}}{8\pi} \right) \mathbf{v} - \frac{1}{4\pi} (\mathbf{v} \cdot \mathbf{B}) \mathbf{B} \end{pmatrix}, \quad (3)$$

$$\mathbf{S} = \begin{pmatrix} 0 \\ \rho \mathbf{g} \\ 0 \\ \rho \mathbf{g} \cdot \mathbf{v} \end{pmatrix}. \quad (4)$$

$\rho$  is the mass density,  $\mathbf{v}$  is the velocity vector,  $\mathbf{B}$  is the magnetic field vector,  $p$  is the gas pressure,  $\mathbf{g}$  is the gravitational acceleration and  $\mathbf{I}$  is the  $3 \times 3$  unit matrix. The total energy  $E$  is given by

$$E = \rho \epsilon + \rho \frac{\mathbf{v} \cdot \mathbf{v}}{2} + \frac{\mathbf{B} \cdot \mathbf{B}}{8\pi}, \quad (5)$$

where  $\epsilon$  is the thermal energy per unit mass. The additional constraint of no magnetic monopoles,

$$\nabla \cdot \mathbf{B} = 0, \quad (6)$$

must also be fulfilled. The MHD equations must be closed by an equation of state which gives the gas pressure as a function of the density and the thermal energy per unit mass

$$p = p(\rho, \epsilon). \quad (7)$$

## 1.2. Spatial and temporal discretization

The magnetohydrodynamic equations are solved on a fixed cartesian grid allowing non-equidistant meshes. The multidimensional problem is reduced to 1-D problems by dimensional splitting. Each of these 1-D problems is solved with a Godunov-type finite-volume scheme using an approximate Riemann solver modified for a general equation of state and gravity. The extension to second order in space and time is done using linear reconstruction for the primitive variables  $\rho$ ,  $v$ ,  $\mathbf{B}$ ,  $p$  and  $\rho\epsilon$  followed by a Hancock predictor step (Toro, 1999).

## 1.3. The Riemann solver

The original hydrodynamics step of CO<sup>5</sup>BOLD uses a Riemann solver of Roe type. For MHD, we decided to use a HLL-solver instead, because the Roe solver does not guarantee the positivity of the density and the pressure. This problem, which may occur also for hydrodynamics, gets worse for MHD. To compute the pressure using the equation of state, Eq. (7), one has to subtract the kinetic and magnetic energy from the total energy, Eq. (5). If the thermal energy is much smaller than the total energy, small errors in the total energy lead to large errors of the thermal energy which may turn the pressure to negative values, especially in regions of strong magnetic field and low plasma beta. Values of  $\beta \approx 10^{-4}$  are common in chromospheric regions.

However, it can be shown, that the HLL solver ensures the positivity of the density and the pressure if the exact solution of the Riemann problem has positive density and pressure (Einfeldt et al., 1991). This is the case for the hydrodynamic equations. For MHD, this is true only if the normal component of the magnetic field has no jump. For 1-D problems, the divergence-free condition forces the normal component of the magnetic field to be constant. For multidimensional problems, jumps in the normal component of the magnetic field are unavoidable using cell centered magnetic fields, even if the divergence-free condition is fulfilled in a discrete sense. It was shown by Janhunen (2000), that allowing magnetic monopoles and taking into account their contribution to the Lorentz-force, an additional source term occurs only in the induction equation. Using a special discretization of this source term, the HLL-solver for the MHD equations is positive (Janhunen, 2000).

## 1.4. The constrained-transport step

A special requirement of MHD-calculations is the enforcement of the divergence-free condition, Eq. (6), for the magnetic field. Violating this condition can lead to unphysical forces which can degrade the solution (Brackbill & Barnes, 1980).

After performing the 1-D substeps, the updated magnetic field is not divergence-free, even if it was before the update. Therefore, an additional step for the update of the magnetic field is required. In our scheme, we use the flux-interpolated constrained transport of Balsara & Spicer (1999). This method uses a staggered grid, where the magnetic fields are stored at the cell boundaries whereas the remaining hydrodynamic variables are located at the cell centers. Because the 1-D updates require magnetic fields located at the cell centers, the magnetic field at the cell centers is computed from the values of the cell boundaries using simple arithmetic averaging. After the 1-D substeps are performed, the updated values of the cell-centered magnetic field are discarded. Instead, the boundary located magnetic field values are updated using the fluxes from the 1-D substeps in such a way, that a discrete version of the divergence-free condition, Eq. (6), is fulfilled.

## 2. FIRST SIMULATIONS

A first three-dimensional magnetohydrodynamic simulation of the integral layers from the upper convection zone to the middle chromosphere was carried out. The computational domain extends over a height range of 2800 km of which 1400 km reach below the mean surface of optical depth unity and 1400 km above it. The horizontal dimensions are  $4800 \times 4800$  km. With  $120^3$  grid cells, the spatial resolution in the horizontal direction is 40 km, while in the vertical direction it is 20 km throughout the photosphere and chromosphere increasing to 50 km through the convection-zone layer. The lateral boundary conditions are periodic in all variables, whereas the lower boundary is “open” in the sense that the fluid can freely flow in and out of the computational domain under the condition of vanishing total mass flux. The specific entropy of the inflowing mass is fixed to a value previously determined so as to yield solar radiative flux at the upper boundary. The upper boundary is “closed” so far, i.e., reflecting boundaries are applied to the vertical velocity, while stress-free conditions are in effect for the horizontal velocities, viz.,  $dv_{x,y}/dz = 0$ . The vertical derivative of the specific internal energy is zero.

The MHD simulation starts with a homogeneous, vertical, unipolar magnetic field of a flux density of 10 G superposed on a previously computed, relaxed model of thermal convection. This flux density ought to mimic magnetoconvection in a network-cell interior. The magnetic field is constrained to have vanishing horizontal components at the top and bottom boundary but lines of

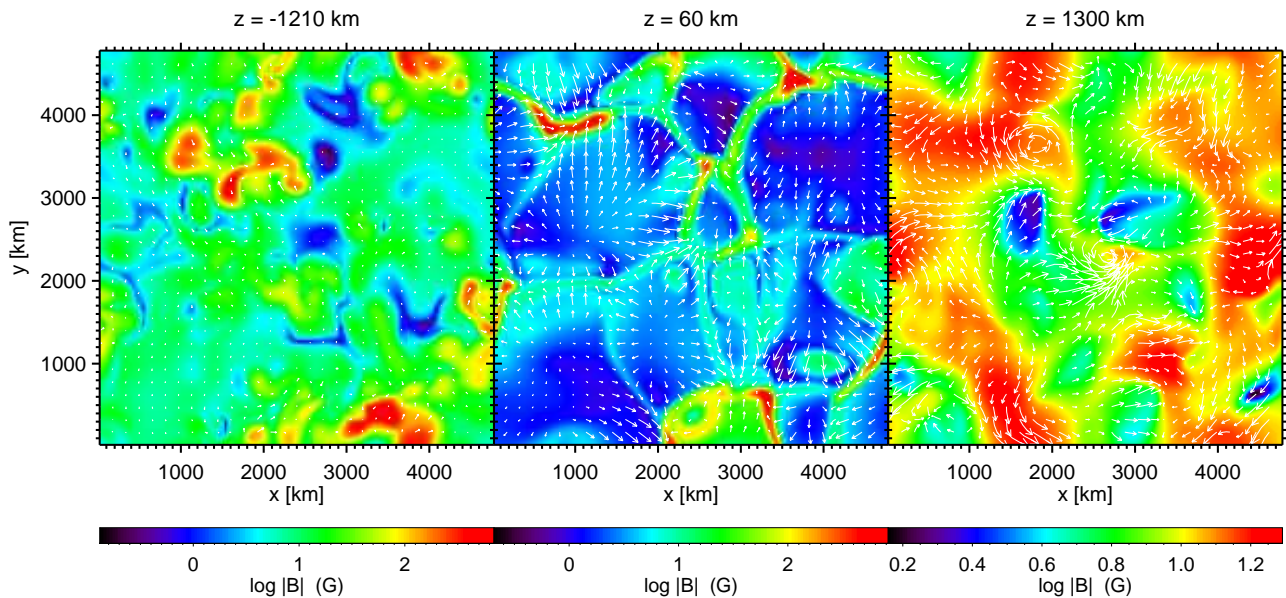


Figure 1. Three horizontal sections through the three-dimensional computational domain. The color coding displays the logarithm of the absolute magnetic field strength, with the individual scalings indicated in the color bars. **Left:** Bottom layer at a depth of 1210 km. **Middle:** Layer 60 km above optical depth  $\tau_c = 1$ . **Right:** Top, chromospheric layer in a height of 1300 km. The white arrows indicate the horizontal component of the velocity field on a common scaling for all three panels. The longest arrows in the panels from left to right correspond to 4.5, 8.8, and 25.2 km/s, respectively.

force can freely move in the horizontal direction, allowing for flux concentrations to extend right to the boundaries. Although this condition is still quite stringent, especially at the top boundary, it allows the magnetic field to freely expand with height through the photospheric layers into the more or less homogeneous chromospheric field, different from conventional simulations that extend to a height of typically 600 km only.

### 2.1. Dynamic chromospheric magnetic field

Subsequent to superposition of the magnetic field, flux expulsion from the granule centers takes place and within less than 5 minutes, the magnetic field concentrates in narrow sheets and small knots near the surface of optical depth unity with field strengths up to approximately 1 kG. Occasionally these magnetic flux concentrations extend down to the bottom boundary at a depth of 1400 km but more often, they disperse again at a depth of less than 1000 km leaving flux concentrations of a strength of a few hundred Gauss only. Fig. 1 shows the logarithm of the absolute magnetic flux density in three horizontal sections through the computational domain at a given time instant.

The left panel refers to a depth of 1210 km, which is close to the bottom boundary, the middle panel to a height of 60 km above the mean surface of optical depth unity, where one can see the horizontal flows that expel the field from the granule centers. The right panel refers to a height of 1300 km, which is located in the chromospheric layers, close to the upper boundary. There, the

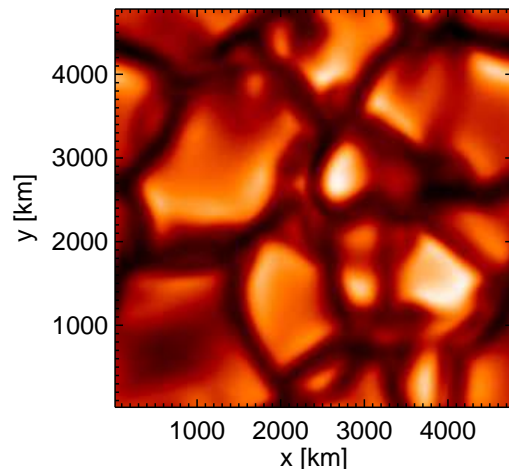


Figure 2. Emergent grey (Rosseland mean) intensity corresponding to the instant of Fig. 1.

magnetic field is marked by strong dynamics with a continuous reshuffling of magnetic flux on a time scale of less than 1 min, much shorter than in the photospheric or convection-zone layers. The field has a strength between 2 and 40 G in this snapshot, which is typical for the whole time series. Different from the surface magnetic field, it is more homogeneous and practically fills the entire space so that the magnetic filling factor in the top layers is close to unity. The formation of weak flux tubes prevails again but on a spatial scale larger than the width of the sheets near the surface. There seems to be no spatial correlation between these chromospheric flux concentrations and the

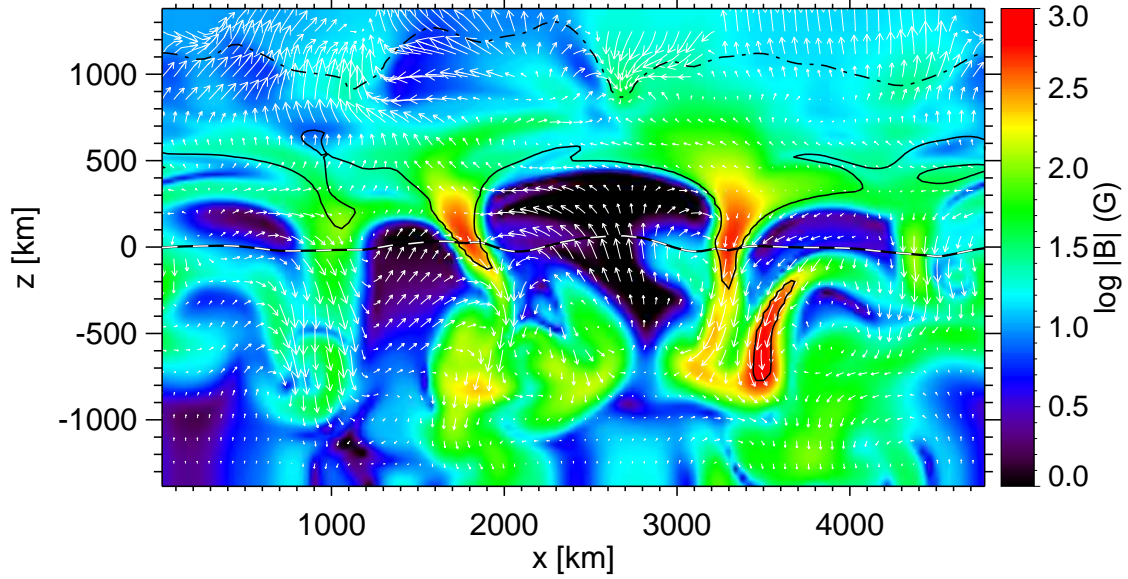


Figure 3. Snapshot of a vertical section showing the logarithm of the absolute field strength (color coded) and velocity vectors projected on the vertical plane (white arrows). The b/w dashed curve shows optical depth unity for vertical lines of sight and the dot-dashed and solid black contours correspond to  $\beta = 1$  and 100, respectively.

small-scale field concentrations in the photosphere. The former rather have a slight tendency to be located in between the flux concentrations at the surface.

Fig. 2 shows the emergent Rosseland mean intensity corresponding to the instant of Fig. 1. Several granules are visible. Comparing the middle panel of Fig. 1 with Fig. 2, one readily sees that the magnetic field is concentrated in intergranular lanes and at lane vertices. However, the field concentrations do not show a corresponding intensity signal. This is because the magnetic flux is too weak to form a significant “Wilson depression” (as can be seen from Figs. 3 and 5) so that no radiative channeling effect can take place.

Fig. 3 shows the logarithm of the absolute field strength (color coded) through a vertical section of the computational domain. Overplotted are white arrows indicating the velocity field. The b/w dashed curve corresponds to the optical depth unity for vertical lines of sight. Contours of the ratio of thermal to magnetic pressure,  $\beta = p_{\text{gas}}/(B^2/2\mu)$  for  $\beta = 1$  (dot-dashed) and  $\beta = 100$  (solid) are also shown. Highly dynamic transient filaments of stronger than average magnetic field are a ubiquitous phenomenon in the chromosphere and are also present in the snapshot of Fig. 3 along the contour of  $\beta = 1$  near  $x = 1000$  km and  $x = 2700$  km. They form in the compression zone downstream and along propagating shock fronts – the latter continue to be an integral part of chromospheric dynamics as already known from the non-magnetic case (Wedemeyer et al., 2004). These magnetic filaments that have a field strength rarely exceeding 40 G, rapidly move with the shock fronts and quickly form and dissolve with them.

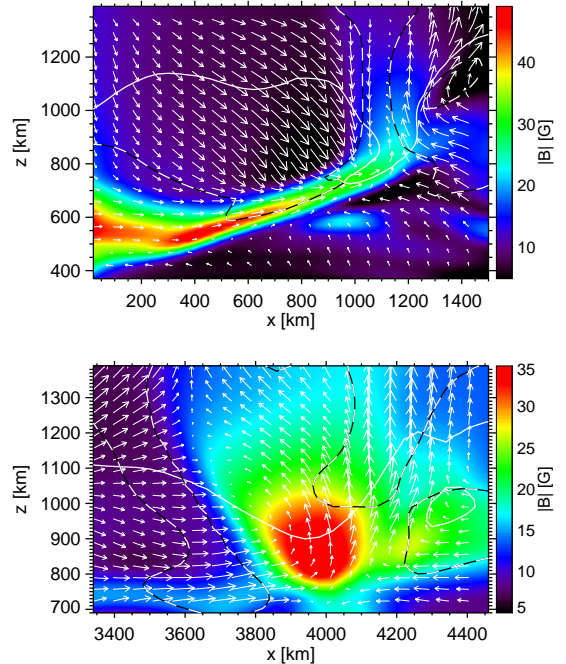


Figure 4. Two instances of shock induced magnetic field compression. Absolute magnetic flux density (colors) with velocity field (arrows), Mach = 1-contour (dashed) and  $\beta = 1$ -contour (white solid).

Fig. 4 shows close-ups of two instances of shock induced magnetic field compression. The absolute magnetic field strength (color coded) is shown together with the velocity field (white arrows), contours of Mach number unity

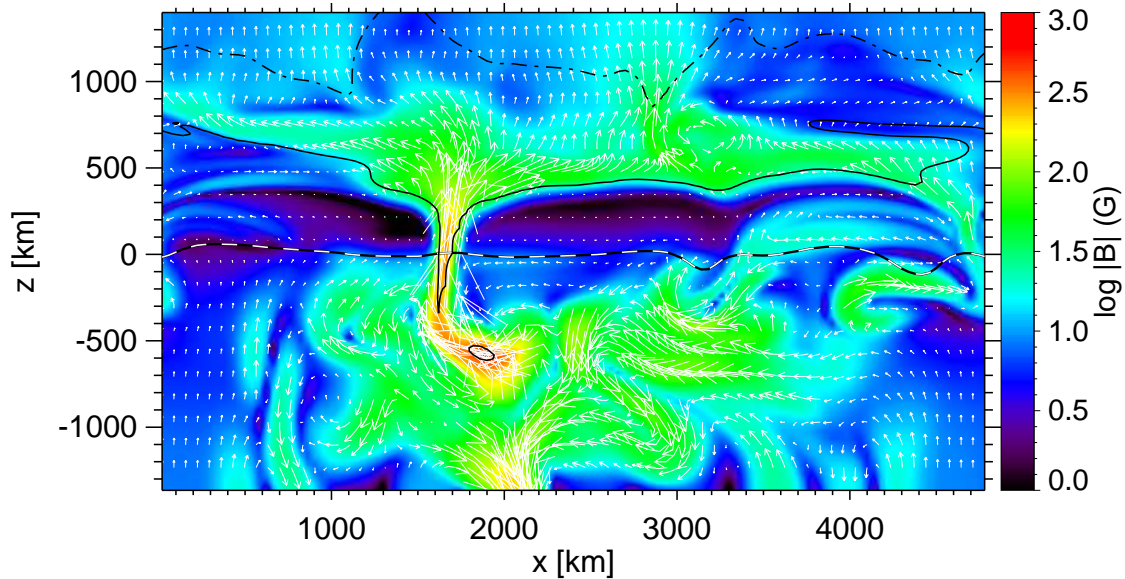


Figure 5. Like Fig. 3 but with the white arrows representing vectors of the magnetic field projected on the vertical plane.

(dashed) and of  $\beta = 1$  (white solid curve). In both cases field has been swept to the region downstream the transition from supersonic to subsonic plasma flow. The surface of  $\beta = 1$  separates the region of highly dynamic magnetic fields from the more slowly evolving field of high beta plasma below it. According to Bogdan, Carlsson & Hansteen et al. (2003), this layer acts as a mode conversion zone, which indeed is observed in the present simulation.

## 2.2. Small-scale canopy fields

Fig. 5 shows the same quantities as Fig. 3 does, but for a different instant and with the exception that the white arrows display the magnetic field projected on the corresponding vertical plane. Like Fig. 3, it nicely exhibits the formation of a “magnetic canopy field” that extends in a more or less horizontal direction over expanding granules and in between photospheric flux concentrations. Visible is also the merging of two neighbouring canopy fields of opposite direction near  $x = 3000$  km, where both fields turn into a more vertical direction. The formation of such canopy fields—a very common phenomenon in the present simulation run—proceeds by action of the horizontally expanding flow above granule centers. This can be seen in Fig. 3 (center), where the arrows indicate the velocity field. Consequently, the canopy field continuously evolves with a time scale of granular life time. The base of the canopy, which harbors weak field with a beta plasma of around 100 is located in a height of 400 km. Note that a similar canopy could not form in previous comparable two and three-dimensional simulations, since they typically have the top boundary located at 600 km, where the field is forced to become vertical.

The absolute magnetic field strength in the “voids” below the canopy field is less than 3 G. This result is still compatible with recent models from Hanle depolarization measurements that predict the “turbulent field” to be organized at the spatial scale of the granulation with very weak fields above the granules (Trujillo Bueno, Shchukina & Asensio Ramos, 2004). The latter result would be compatible with the present simulation if referring to the field above the canopy in the top photosphere and chromosphere. Note that like Fig. 3, also Fig. 5 shows the characteristic filaments in field strength in the chromospheric layers close to the surface of equal thermal and magnetic pressure,  $\beta = 1$ .

## 3. CONCLUSIONS

The hydrodynamic code CO<sup>5</sup>BOLD has been extended to magnetohydrodynamics using a 2nd order accurate HLL Riemann solver for computing the numerical fluxes and a constrained transport for divergence free transport of the magnetic field.

A first three-dimensional magnetohydrodynamic simulation of the integral layers from the convection zone to the chromosphere has been carried out. The simulation is intended to represent magnetoconvection in a quiet network-cell interior. It reveals a chromospheric magnetic field that is strongly dynamic. There, the magnetic field is continuously rearranged on a time scale of less than 1 min. This is the expression of rapidly moving, transient magnetic filaments that form in the compression zone downstream and along propagating shock fronts. These filaments that have a field strength that is stronger than the average but rarely exceeding 40 G,

move with the shock waves and quickly form and dissolve with them. The surface of  $\beta = 1$  separates the region of highly dynamic magnetic fields from the more slowly evolving field of high beta plasma below it and seems to act as a wave conversion zone. This surface is located at approximately 1000 km but it is corrugated and its height strongly varies in time.

The magnetic field gets almost completely expelled from the photospheric layers of granule interiors, leading to a horizontally directed but continuously changing “canopy field” that overlays these “voids”. This result possibly contradicts the ideal model of a space filling turbulent weak field in the photosphere, customarily used for the interpretation of Hanle depolarization measurements. Over all, the picture of flux concentrations that strongly expand through the photosphere into a more homogeneous, space filling chromospheric field (Solanki & Steiner, 1990) remains valid.

## ACKNOWLEDGMENTS

WS was supported by the Austrian *Fonds zur Förderung der Wissenschaften* through the Erwin Schrödinger Stipendium, project J2211. SW acknowledges support by the *Deutsche Forschungsgemeinschaft (DFG)*, project Ste 615/5.

## REFERENCES

- Balsara, D. S. & Spicer, D. S., 1999, A Staggered Mesh Algorithm Using High Order Godunov Fluxes to Ensure Solenoidal Magnetic Fields in Magnetohydrodynamic Simulations, *J. Comput. Phys.*, 149, 270
- Bogdan, T. J., Carlsson, M., Hansteen, V. H., McMurry, A., Rosenthal, C. S., Johnson, M., Petty-Powell, S., Zita, E. J., Stein, R. F., McIntosh, S. W. & Nordlund, Å., 2003, Waves in the Magnetized Solar Atmosphere. II. Waves from Localized Sources in Magnetic Flux Concentrations, *ApJ*, 599, 626
- Brackbill, J. U. & Barnes, D. C., 1980, The effect of nonzero  $\nabla \cdot \mathbf{B}$  on the numerical solution of the magnetohydrodynamic equations, *J. Comput. Phys.*, 35, 426
- Einfeldt, B., Munz C. D., Roe, P. L. & Sjögren, B., 1991, On Godunov-type methods near low densities, *J. Comput. Phys.*, 92, 273
- Janhunen P., 2000, A Positive Conservative Method for Magnetohydrodynamics Based on HLL and Roe Methods, *J. Comput. Phys.*, 160, 649
- Solanki, S. K. & Steiner, O., How magnetic is the solar chromosphere?, 1990, *A&A*, 234, 519
- Toro, E. F., 1999, *Riemann Solvers and Numerical Methods for Fluid Dynamics a Practical Introduction*, Springer Berlin-Heidelberg
- Trujillo Bueno, J., Shchukina, N. & Asensio Ramos, A., 2004, A substantial amount of hidden magnetic energy in the quiet Sun, *Nature*, 430, 326

Wedemeyer, S., Freytag, B., Steffen, M., Ludwig, H.-G. & Holweger, H., 2004, Numerical simulation of the three-dimensional structure and dynamics of the non-magnetic solar chromosphere, *A&A*, 414, 1121